RSC Advances

PAPER

View Article Online
View Journal | View Issue

Cite this: *RSC Adv.*, 2021, **11**, 34193

Towards the development of flexible carbon nanotube–parafilm nanocomposites and their application as bioelectrodes†

N. Gopal,[a] S. Kumar[b] and R. Sahney *[a]

Soft, flexible and conductive interfaces, which can be used as electrode materials integrated with commercial electronic components and the human body for continuous monitoring of different analytes are in high demand in wearable electronics. In the present work, we explore the development of a functionalized multi-walled carbon nanotube‡–parafilm§ nanocomposite (f-MWCNT–PF) for the fabrication of a flexible electrochemical platform for glucose detection. The f-MWCNT–PF nanocomposite was characterized by transmission electron microscopy, energy dispersive X-ray analysis, Fourier-transform infrared spectroscopy, Raman spectroscopy, and electrochemical techniques. A bioelectrode fabricated by immobilization of glucose oxidase at the f-MWCNT–PF surface was further characterized by atomic force microscopy and tested for glucose. The bioelectrode provides two linear regions of glucose detection: a linear range from 0.08 mM to 3 mM, with a correlation coefficient of 0.982 and a sensitivity of 35.322 μA mM^{-1}; and a linear range from 5 mM to 25 mM, with a correlation coefficient of 0.964 and a sensitivity of 9.346 μA mM^{-1}. The proposed method was successfully applied to measure glucose in blood serum samples, differentiating healthy and diabetic persons. Additionally, the lower detection region could be effectively applicable for glucose sensing in sweat or interstitial fluid samples. The flexible, water-repellant sensing platform can be used as a universal platform for analyte detection, demanding waterproof, conductive platforms for biosensing applications, as it is suitable for protein/enzyme immobilization.

Received 8th March 2021
Accepted 21st September 2021

DOI: 10.1039/d1ra01840j

rsc.li/rsc-advances

1. Introduction

Biomolecules such as proteins and DNA are attractive building blocks for molecular-scale devices/nanodevices in which biomolecules and electronic elements are integrated into functional systems.[1] Hybrid systems formed by the integration of biomolecules with electronic elements such as electrodes or transistors enable the electronic readout detection of biomolecular functions, the transformation of biocatalyzed processes into electrical power, and the templating of nanosized circuitry.[2] Electron transfer between biomolecules and electronic elements such as electrodes is the hallmark of biomolecular systems and the construction of biosensors.[3] Nevertheless, electrode units and biomolecules lack natural communication.[4] Therefore, the structural design of biomolecular architectures on electronic support is needed to facilitate communication between the components so that biological events can be transduced into electronic signals.[5] Our group has reported the fabrication of an electrode for urea sensing using a glass pH electrode[6,7] and cholesterol measurement using liquid membrane-based sensors,[8] demonstrating the potential application of hybrid systems in clinical applications. Glassy carbon electrode modified with nickel oxide (NiO)-decorated molybdenum disulfide (MoS_2) nanosheets and $MoSe_2$ nanosheets-decorated nickel oxide (NiO) nanorods have also been used for the fabrication of non-enzymatic glucose sensors.[9,10] To meet the ever-increasing demands for new and efficient electrochemical platforms, stretchable conductive composites are promising electrode materials for electrochemical biosensor fabrication.[11] In particular, multi-walled carbon nanotubes (MWCNT), when paired with a polymeric matrix, offer a hybrid material system that can be tailored for many high-value applications in addition to being sustainable.[12–14] The conducting π-conjugative structure and hydrophobic surface of CNTs allows them to form new composites and films, which have been used in designing many nanodevices and biosensors.[15] The advantageous properties of MWCNT exploited for the development of new hybrid systems include high electrical conductivity,[16] impressive mechanical and thermal stability,[17] flexibility of modulating the specific surface

[a]*Amity Institute of Biotechnology, AUUP, Noida, India-201303. E-mail: rachanasahney@gmail.com; rsahney@amity.edu; Fax: +91 120 2431878; Tel: +91 120 2432780 85*

[b]*St. Stephens College, Delhi University, New Delhi, India*

† Electronic supplementary information (ESI) available. See DOI: 10.1039/d1ra01840j

‡ Functionalized multi-walled carbon nanotube (f-MWCNT).

§ Parafilm-M (PF).

area (50 to 500 m^2 g^{-1} with internal diameters from 5 to 100 nm),[18] and the possibility of shaping the macroscopic morphology of the support.[19] Other attractive features of MWCNTs used for the development of new materials are the possibility of fine-tuning the specific metal–support interactions,[20,21] the flexibility of functionalizing the surfaces and thus changing the hydrophilicity, pH, electron donor–acceptor properties, and specific chemical properties of the surface[22,23] that are more resistant to changes by aqueous hydrolytic effects compared to other conventional support materials, such as silica.

For a seamless integration of rigid MWCNT on polymeric supports, innovative polymeric materials with stretchable and hydrophobic properties are advantageous for many electronics applications,[24] such as flexible energy storage, wearable electronics, and printable circuitry. Different techniques have been exploited for the development of CNT–polymer nanocomposites with multifunctional properties by transferring the excellent electrical properties of CNTs to insulating polymer matrices.[25]

Paraffin wax doped with various carbon-based materials has been used for thermal energy storage, enhanced heat transfer application, and electrochemical sensing.[26–28] But the scalable single-step fabrication of flexible sheet-type composite electrodes, which can have significant advantages for practical application in wearable biosensors, has not been reported. Parafilm-M (PF) is a blended thermoplastic film containing paraffin wax and polyolefin as constituents.[29] It is soft, stretchable, non-toxic, and semi-transparent.[30,31] PF has found applications in plants for grafting scaffolds,[32] as a source for *n*-alkane standards in gas chromatography,[33] and in analytical devices,[34] reduction of dental plaque formation[35] and biopsy-tissue preservation. Owing to its low melting point,[29] it becomes adhesive on heating and sticks strongly to the receiving material. Elastomeric films of graphene nanoplates/PF laminated on fluoroelastomers show anti-corrosive behavior and can be used as valuable packaging films,[36] while combining PF with carbon nanofibers affords elastomeric conductive composites capable of sustaining severe elastic deformation with uncompromised hydrophobicity and recoverable electrical performance.[37] The self-sticking feature of PF is useful for the large production of stretchable multifunctional materials.

In the present study, we aim to develop a f-MWCNT–PF nanocomposite electrode as a universal conductive platform that can be used for immobilization of enzymes or antibodies. We show that once CNT is transferred to the self-adherent PF, it can be used for the development of biosensors. We employ glucose oxidase (GOx) as a model enzyme for the evaluation of the biosensing function of a universal electrochemical platform for sensing glucose. Our study suggests new directions for fabricating sheet-type electrodes for biosensing applications in future biomedical devices.

2. Experimental

2.1 Materials

Pristine multiwalled carbon nanotubes (p-MWCNTs) with average dimensions for individual MWCNTs of 10–30 nm in diameter and 0.2–2.00 μm in length were purchased from Chengdu Organic Chemistry Co. Ltd. Parafilm M (PF), Product Number P 7793, and potassium ferricyanide were obtained from Sigma-Aldrich. 1-(3-Dimethylaminopropyl)-3-ethyl carbodiimide hydrochloride (EDC), *N*-hydroxysulfosuccinimide (NHS), and GOx were supplied by Sisco Research Laboratory Pvt. Ltd (SRL). All other chemicals used in the experiments were supplied by Merck, India. Double-distilled water was used throughout the experiments.

2.2 Functionalization of p-MWCNT and bio-electrode fabrication

Chemical oxidation of p-MWCNTs was performed with a mixture of H_2SO_4 and HNO_3 (3 : 1 v/v) in a round-bottomed flask at 60 °C for 6 h.[38]

The f-MWCNTs (50 mg) so obtained were placed in a glass bottle (15 mL), and 1.0 mL of ethanol was added at intervals of one hour while continuously sonicating the mixture for 10 h. The resulting f-MWCNT-ink was transferred to a glass slide (6×2 cm^2) using the doctor's blade method.[39] The film was dried overnight at room temperature. A piece of PF (6×2 cm^2) was cast over a f-MWCNT film spread on the glass plate and heated on the hot plate at a constant temperature (65 °C) to form a nanocomposite film. Finally, the f-MWCNT–PF was cut into small pieces. It was directly used for various studies and as working electrodes.

The amount of surface carboxylic functions present at f-MWCNT and f-MWCNT–PF were determined by the Boehm titration method.[40] EDC–NHS chemistry[41] was used to immobilize GOx at the surface of the f-MWCNT–PF nanocomposite with carboxylic functional groups to develop a GOx–f-MWCNT–PF nanocomposite film. Washed nanocomposite films were directly used for the determination of enzyme activity, in stability studies, and as a working electrode.

2.3 Characterization

The morphologies of the MWCNTs and nanocomposites were characterized by transmission electron microscopy (TEM; Tecnai g2T30). The elemental composition of different samples was determined using a Zeiss EVO 50 scanning electron microscope (SEM) coupled with energy dispersive X-ray analysis (EDX) equipment. Fourier transform infra-red (FTIR) spectra were recorded in transmission mode using a Perkin-Elmer spectrometer (Model: Spectrum RXI – Mid IR) in the spectral range from 4000 to 500 cm^{-1}. Raman spectra were recorded using a 532 nm excitation laser beam (Varian FT-Raman 600 UMA). Surface immobilization of GOx at the surface of the f-MWCNT–PF nanocomposite was studied using atomic force microscopy (AFM) with a Solver NT-MDT probe in contact mode.

2.4 Electrochemical measurements

Electrochemical measurements were performed with a potentiostat (Gamry Interface 1000, USA) using a conventional three-electrode setup consisting of a working electrode (f-MWCNT–PF nanocomposite/GOx–f-MWCNT–PF nanocomposite electrode), Ag/AgCl as a reference electrode, and a platinum wire as a counter electrode. All measurements were performed in 5.0 mL of an aqueous solution containing 5 mM $K_3[Fe(CN)_6]$ (5 mM), 0.1 M KCl, and 0.1 M sodium phosphate buffer at pH 7.4.

The immobilization of GOx on the f-MWCNT–PF nanocomposite electrode was characterized by electrochemical impedance spectroscopy (EIS). The alternating voltage used for measurement was 10 mV, and the frequency range was 0.2 Hz to 1.0 MHz. The concentrations of β-D-glucose solution were measured by the standard addition method using voltammetry, and a calibration curve was obtained. Glucose measurements in blood serum samples (anonymized) obtained from the hospital were performed by using 10 μL of the sample in the same buffer medium as above. GOx–f-MWCNT–PF nanocomposite electrodes were stored in phosphate buffer at 4 °C in a refrigerator when not in use.

Details of the experimental methods are given in the ESI data file as S1.†

3. Results and discussion

3.1 Preparation of a flexible glucose sensor with the f-MWCNT–PF nanocomposite

The schematic fabrication process of the flexible glucose sensor using f-MWCNT and thermoplastic PF is illustrated in Fig. 1. The overall steps include (i) functionalization of p-MWCNT by chemical oxidation, (ii) stable dispersion of f-MWCNT in ethanol to form a homogeneous CNT-ink, (iii) f-MWCNT ink casting on a glass slide manually by the doctor's blade method and drying at room temperature (8 h) in the air, (iv) PF casting on the dried CNT-ink platform and simultaneous thermal transfer of f-MWCNT onto the PF surface by heating at 65 °C to form the f-MWCNT–PF nanocomposite film, (v) immobilization of GOx on the nanocomposite surface to produce the GOx–f-MWCNT–PF nanocomposite film, which is directly used as the working electrode, and (vi) electrochemical measurements using the glucose-sensitive electrode (bioelectrode).

The f-MWCNT–PF nanocomposite film was designed to fabricate a new flexible electrode by transferring the unique electrical properties of rigid nanotubes to the rather insulating PF matrix. The nanocomposite fabrication was achieved by casting PF at the f-MWCNT layer on the glass slide; therefore, the density of MWCNT on the MWCNT-rich side of our film is higher. The strong sticking behavior of PF at low temperature allows embedding of f-MWCNT in the PF, forming f-MWCNT–

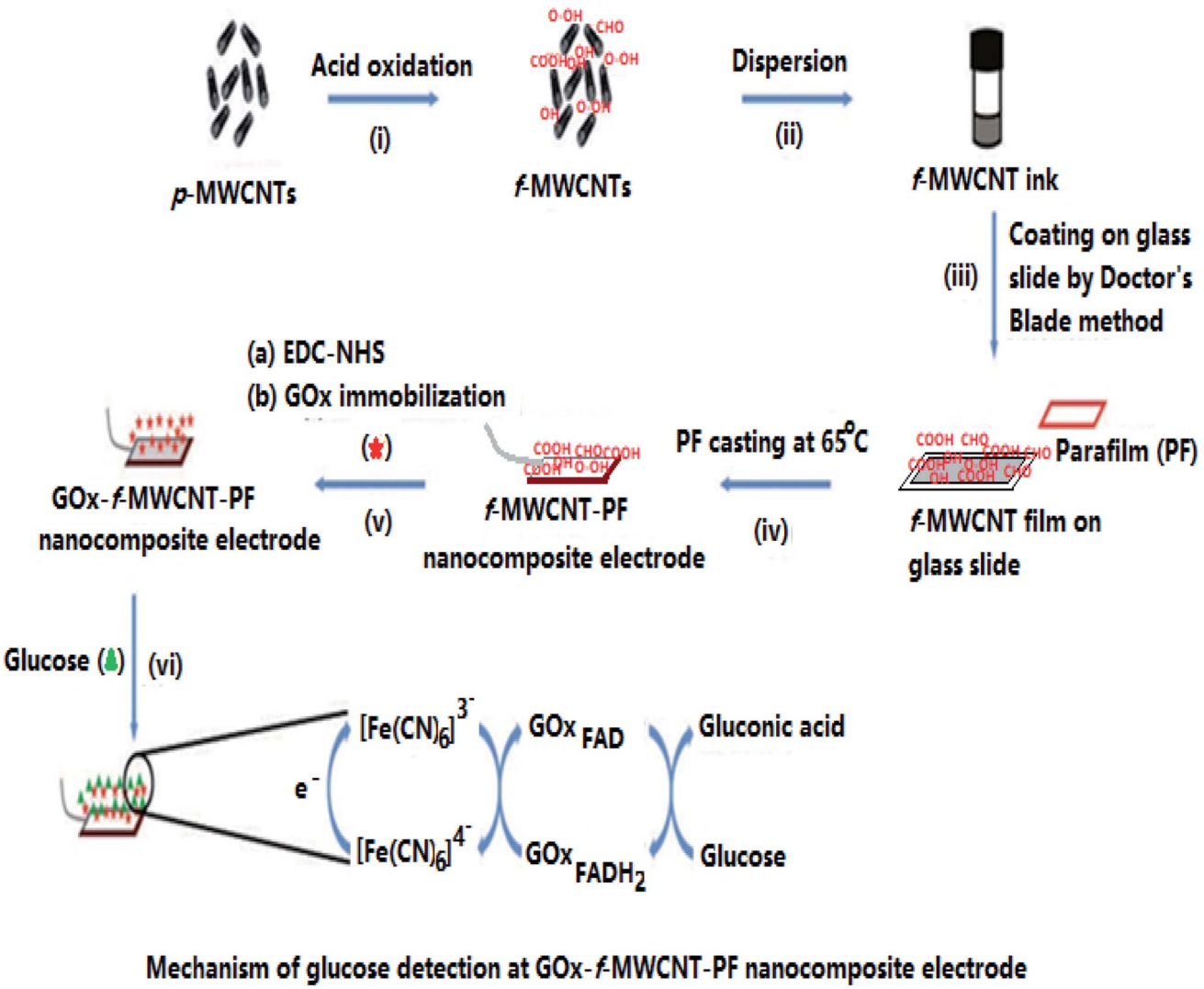

Fig. 1 Schematic of the steps involved in the fabrication of the f-MWCNT–PF nanocomposite-based glucose biosensor.

PF nanocomposites. The possibility to achieve reasonably high conductivity at low CNT content owing to its high aspect ratio (L/D, where L is the length and D is the diameter of the CNTs) makes them an ideal candidate for several potential applications.[42–44] Their high aspect ratio enables CNTs to form a 'network-like' structure in the composites at a particular, often low concentration, a phenomenon termed 'percolation'.[45]

Usually, CNTs are entwined with each other by hydrophobic van der Waals forces and dispersed as aggregates in a polymeric matrix, which limits their applications in biomolecule immobilization and sensor fabrication. Strategically, acid treatment (HNO_3/H_2SO_4) was applied to fine-tune the surface properties of p-MWCNT for enzyme immobilization.[37] The oxidation process generates several hydrophilic groups at the CNT surface, but carboxyl functions are most pertinent[46] for enzyme/protein immobilization. These acidic oxygen groups at the nanotube surface can interact with the amine groups of the protein chains from the enzyme, allowing strong interactions by the formation of amide bridges.[47] This implies that the surface carboxyl function governs the enzyme content at the sensing surface. Thus, Boehm titration[40] was applied to determine the effectiveness of the oxidation process for enzyme immobilization, as reported earlier.[48] The potentiometric quantification of surface carboxylic groups attained in the f-MWCNT and f-MWCNT–PF nanocomposite films is 1.3009 mmol g^{-1} of MWCNT and 1.1466 mmol g^{-1}, respectively (details are given in the ESI data file as S2†). The partial hydrophilic nature of f-MWCNT allowed us to produce a CNT-ink in ethanol, which is a non-corrosive solvent to the human body. The CNT ink transferred onto a glass slide exhibited outstanding adhesion.

The maximum amount of CNT filler that can be homogeneously incorporated in a polymeric host is limited. For electrochemical sensor applications, the electrical properties of the f-MWCNT–PF nanocomposite are important. These can be controlled by the MWCNT content and its dispersion in the PF matrix. Thus, different f-MWCNT–PF nanocomposites were prepared with varying CNT content. The cyclic voltammetry was performed at a scan rate of 50 mV s^{-1} between the potentials of ±1.0 V. Nanocomposite electrodes with large, reproducible peak current (I_p), accompanied by the smallest difference in peak potential (ΔE_p) and no visible cracks at the electrode surface, were chosen as working electrodes for sensor fabrication. Thus, in our experiments, a nanocomposite film containing 0.01589 g of f-MWCNT per gram of PF (1.58% wt) was chosen as the electrode material (f-MWCNT–PF nanocomposite electrode) for further studies, as it showed uniform dispersion of CNTs in PF with reproducible electrical properties.

3.2 Characterization by TEM and EDX

Oxidation of nanotubes and sonication in ethanol affects the morphology, size, and dispersion of f-MWCNT in ethanol.[49,50] Thus, we used TEM to study the surface morphology of f-MWCNT and compared it with the morphology of p-MWCNT to verify the occurrence of oxidation-induced transformations at the CNT surface and the distribution of f-MWCNT in the PF matrix (Fig. 2a–c). A comparison of Fig. 2a and b shows that p-MWCNTs (as supplied) are in the form of heavily entangled bundles bound together by van der Waals forces, while the f-MWCNTs are more segregated from each other due to the formation of hydrophilic functional groups, breaking the van der Waals attraction between the tubes.[51] The oxidation of p-MWCNT creates varied hydrophilic functionalities, which appear as multiple darker notches at the f-MWCNT surfaces, representing points of functionalization/oxidation.[52,53] Some tubes are broken and have jagged ends, indicating degradation of the tubular structure of the MWCNTs under strongly oxidizing conditions.[38] However, the core diameter of f-MWCNT remains intact, *i.e.*, 5 nm in p-MWCNTs, as determined from the TEM images. Thus, it is evident that surface functionalization was achieved without significant damage to the CNT core structure.

In the present study, a homogeneous f-MWCNT-ink in ethanol was used to construct the MWCNT–PF nanocomposite. A micrograph of the f-MWCNT–PF nanocomposite (Fig. 2c) shows a homogeneous distribution of f-MWCNTs in PF with clear tubular structures intertwined with each other, suggesting the possible formation of a 3D interconnected nanotube network.

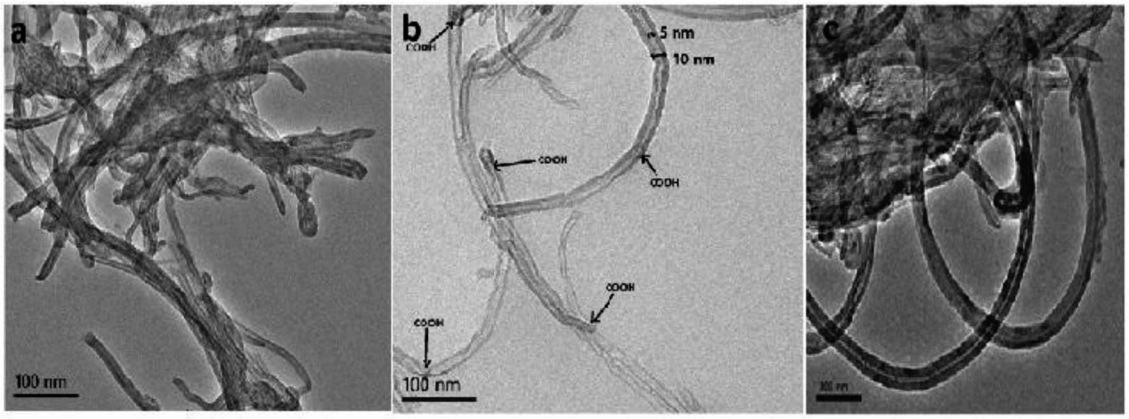

Fig. 2 TEM images of (a) p-MWCNT, (b) f-MWCNT (disentangled) and (c) the f-MWCNT–PF nanocomposite.

The elemental compositions of CNTs and nanocomposite were studied by energy-dispersive X-ray analysis. The EDX data shown in Table 1 reveal that p-MWCNT contains carbon (99.06 wt%). f-MWCNT has a lower weight percent of carbon (91.18 wt%) and higher weight percent of oxygen (8.65 wt%), suggesting oxidation of the p-MWCNT surface and formation of oxygen-based functionalities at the nanotube surface (–COOH, –OH).[52] The absence of an oxygen peak in the case of p-MWCNT may be due to the presence of vacuum conditions applied during the EDX measurement. The presence of trace amounts of Ni and Pd suggests that the metal impurities are introduced during CNT synthesis at the manufacturer's level (EDAX images are given in the ESI data file as S3†). The decrease in oxygen content (wt%) after nanocomposite formation could be due to amalgamation of the MWCNTs in the parafilm matrix containing paraffin wax and polyolefins, which are hydrocarbons.

3.3 Chemical group analysis by FTIR spectroscopy

The FTIR spectrum of p-MWCNT (as received) is shown in Fig. 3a. The almost featureless, very low intensity IR spectrum obtained is characteristic of the sp^2 carbon present in CNTs. However, the oxidation treatment leads to the appearance of new bands with comparatively high intensity, as shown in Fig. 3b, with peaks at 3468 cm^{-1} (O–H stretching vibration), 1600 cm^{-1} (conjugated C=C stretching), 1731 cm^{-1} (C=O stretching in carboxylic acid) and 1384 cm^{-1} (C–H stretching vibration). After the transfer of f-MWCNTs to the PF surface by heating at 65 °C, the FTIR spectrum undergoes variation, as shown in Fig. 3c. The thermoplastic film parafilm contains paraffin wax and polyolefins. The IR spectrum of the nanocomposite exhibits a broad band at about 3462 cm^{-1}, indicating the presence of an O–H bond. The absorption bands at 2934 cm^{-1} and 2378 cm^{-1} are the prominent and characteristic bands for C–H stretching vibration and the hydrocarbon chains of paraffin wax present in PF.[54,55] Besides, the spectrum of the f-MWCNT–PF nanocomposite sample shows vibration bands characteristic of the polyolefins present in PF as a sharp peak at 1662 cm^{-1}, assigned to the overlap of C=C and C=O, and at 1110 cm^{-1}, assigned to the –C–O–C– group.[56] These results confirm that the characteristics of f-MWCNT and PF were incorporated in the nanocomposite.

Table 1 EDX data showing the elemental compositions of p-MWCNT, f-MWCNT, and the f-MWCNT–PF nanocomposite

	Weight%		
Element	p-MWCNT	f-MWCNT	f-MWCNT–PF nanocomposite
C	99.06	91.18	90.44
Cl	0.27	0.09	—
Ni	0.67	0.08	0.42
O	—	8.65	0.86
Pd	—	—	1.62
Au			6.66

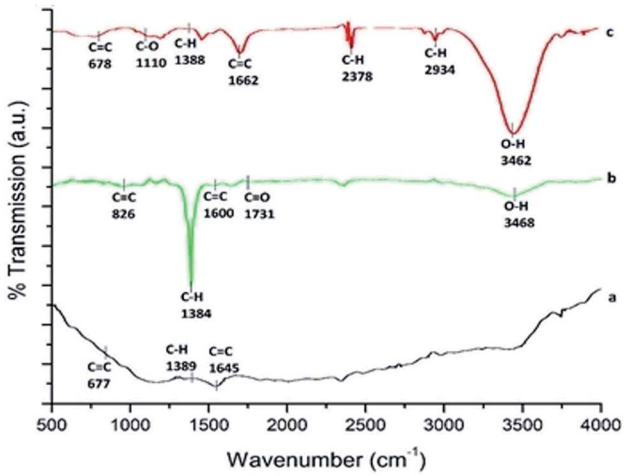

Fig. 3 FTIR spectra of (a) p-MWCNT, (b) f-MWCNT and (c) the f-MWCNT–PF nanocomposite.

3.4 Raman spectroscopic study of MWCNT and the f-MWCNT–PF nanocomposite

Surface functionalization of MWCNTs causes lattice defects in CNTs, which can be detected by Raman spectroscopy.[57] Fig. 4a–c shows the Raman spectra of p-MWCNT, f-MWCNT, and the f-MWCNT–PF nanocomposite, respectively. In these spectra, the D-mode is the disorder band located between 1349–1353 cm^{-1}, the G band is the tangential (vibrations along the tube axis) stretching mode (1500–1600 cm^{-1}) and the G* band is the second-order overtone of the D band, appearing between 2690 and 2715 cm^{-1}. The intensity ratio of the D-band to the G-band (I_D/I_G) reflects both the purity and the defect density of CNTs.[58] A comparison of the Raman spectra of the p-MWCNT, f-MWCNT and f-MWCNT–PF nanocomposites shows that the D, G and G* bands are present (Fig. 4a–c) at similar wavenumbers, but their intensities are different. The I_D/I_G ratio increases when

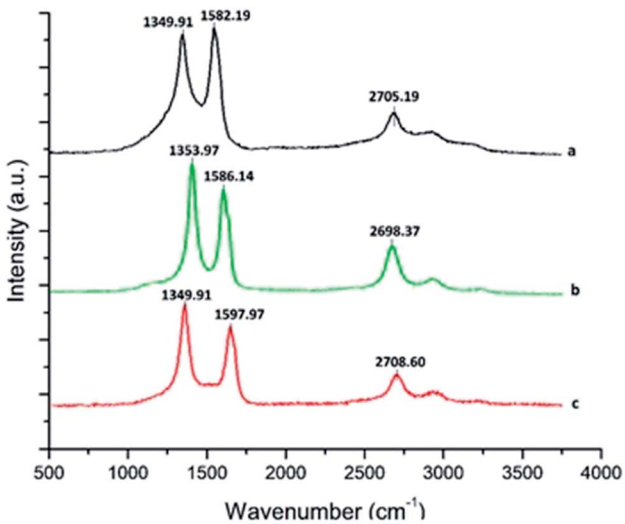

Fig. 4 Raman spectra of (a) p-MWCNT, (b) f-MWCNT and (c) the f-MWCNT–PF nanocomposite.

p-MWCNT (I_D/I_G = 0.9706) is oxidized to f-MWCNT (I_D/I_G = 1.0415) and further added as filler to form the f-MWCNT–PF nanocomposite (I_D/I_G = 1.0669). Thus, the chemical oxidation process is less corrosive to the sp^2 carbon present in CNTs. Nanocomposite film synthesis does not aggressively disrupt the structure of the CNTs.

3.5 Electrode assembly and characterization by AFM

A f-MWCNT–PF nanocomposite electrode with fixed geometrical dimensions (5 mm × 2 mm) was used to immobilize GOx through EDC–NHS coupling reactions and enable the development of a bioelectrode (GOx–f-MWCNT–PF nanocomposite electrode). AFM is an important tool to study the surface features and the immobilization of biomolecules at the microscale.[59,60] The nano-features of the f-MWCNT–PF and GOx–f-MWCNT–PF nanocomposites can be distinguished in the AFM images, which represent both a two- and three-dimensional reconstruction of the surface topography measured across a 1 μm^2 square pattern. The AFM images (Fig. 5a–d) show the micro-morphology and roughness of the f-MWCNT–PF (Fig. 5a and b) and GOx–f-MWCNT–PF (Fig. 5c and d) nanocomposites. A network of MWCNT tubes can be observed on the surface in Fig. 5a and b. The CNTs are dispersed uniformly in the f-MWCNT–PF and GOx–f-MWCNT–PF nanocomposites, and no apparent aggregation can be seen in the images. Thus, it can be presumed that the intrinsic molecular chains are locally disordered in PF on heating, and an interpenetrating structure between the polymer and CNT phases exists due to the thermoplastic behavior of PF. The f-MWCNT–PF nanocomposite has a comparatively smooth surface, with a roughness (RMS) value of 32.4 nm. The immobilization of GOx on the f-MWCNT–PF nanocomposite surface by EDC–NHS chemistry leads to an increase in the roughness value of the GOx–f-MWCNT–PF nanocomposite film (RMS = 59 nm), suggesting deposition of GOx molecules at the nanocomposite film surface.

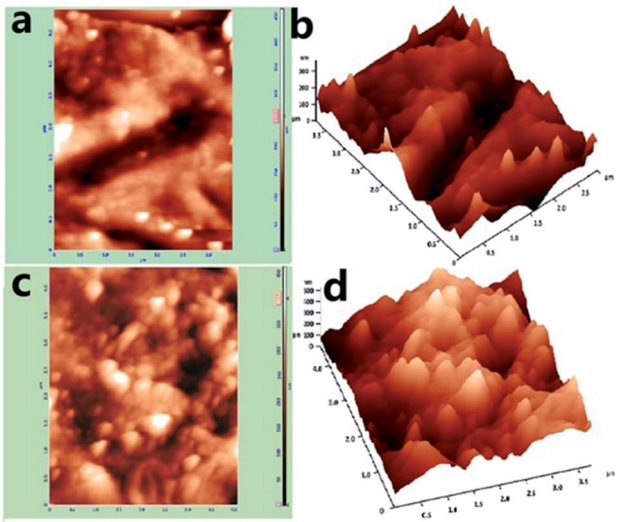

Fig. 5 AFM images: (a) f-MWCNT–PF nanocomposite (2D), (b) f-MWCNT–PF nanocomposite (3D), (c) GOx–f-MWCNT–PF nanocomposite (2D), (d) GOx–f-MWCNT–PF nanocomposite (3D).

3.6 Electrochemical studies of the MWCNT–PF nanocomposite electrodes

3.6.1 Voltametric measurements of GCE, the f-MWCNT–PF nanocomposite electrode, and the GOx–f-MWCNT–PF nanocomposite electrode. Cyclic voltammetry was used to evaluate the sensing responses of the electrodes at different assembly stages. Electrochemical characterization of the f-MWCNT–PF and GOx–f-MWCNT–PF nanocomposite electrodes revealed their basic electrode properties and potential for bioanalytical application. Fig. 6a, b and c show cyclic voltammograms obtained from a bare glassy carbon electrode (GCE), f-MWCNT–PF nanocomposite electrode and GOx–f-MWCNT–PF nanocomposite electrode, respectively, in a phosphate buffer solution containing 5 mM $K_3[Fe(CN)_6]$ with 0.1 M KCl at a scan rate of 50 mV s^{-1}. A pair of well-defined redox peaks were observed for each electrode, with considerable differences in the peak heights. Both the CNT electrodes show higher anodic peak current (I_{pa}) and cathodic peak current (I_{pc}) as compared to GCE; this confirms their excellent electrical conductivity, which is beneficial for promoting electrochemical studies.[61,62] The GOx–f-MWCNT–PF nanocomposite electrode shows lower peak currents (I_{pa} and I_{pc}) than the f-MWCNT–PF nanocomposite electrode due to covalent immobilization of GOx at the electrode surface, which acts as a barrier that inhibits electron transfer at the CNT surface.[63] The f-MWCNT–PF nanocomposite electrode shows a higher charging current, as dissociation of the surface carboxylic groups occurs at pH 7.4 in the buffer solution. Thus, the presence of surface carboxylic groups improves the electron transport behavior at the f-MWCNT–PF nanocomposite electrode surface.[61] The effective surface area of the working electrode (f-MWCNT–PF nanocomposite electrode) was evaluated with the Randles–Sevcik equation using $K_3Fe(CN)_6/K_4Fe(CN)_6$ as an indicator.[64]

$$I_p = (2.687 \times 10^5) n^{3/2} \nu^{1/2} D^{1/2} A C$$

where $n = 1$, ν is the scan rate (V s^{-1}), $D = 7.17 \times 10^{-6}$ cm^2 s^{-1}, and C is the concentration (mol cm^{-3}) of $K_3[Fe(CN)_6]$. The

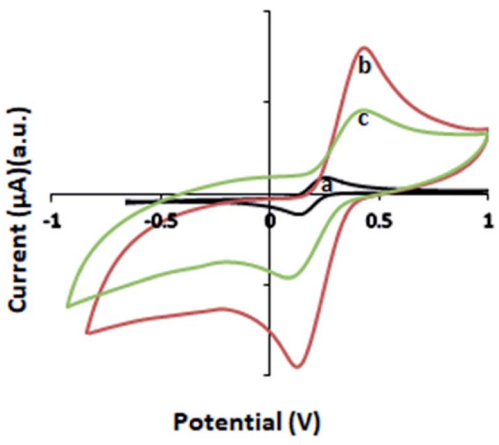

Fig. 6 Comparative cyclic voltammetric responses of the electrodes at a scan rate of 50 mV s^{-1}: (a) GCE, (b) the f-MWCNT–PF nanocomposite electrode and (c) the GOx–f-MWCNT–PF nanocomposite bioelectrode in 5 mM $K_3[Fe(CN)_6]$ with 0.1 M KCl solution.

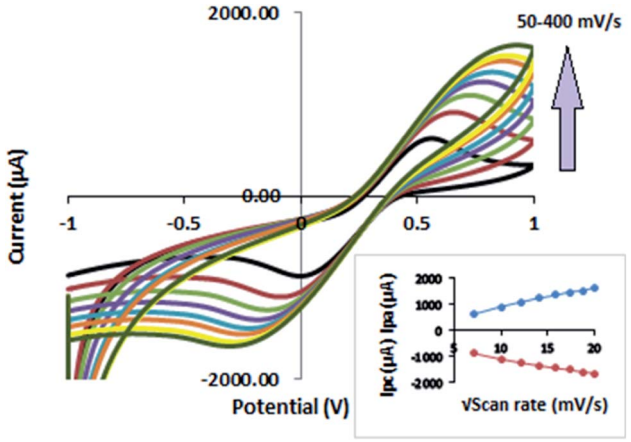

Fig. 7 Overlaid cyclic voltammograms of the f-MWCNT–PF nanocomposite electrode recorded at different scan rates ranging from 50 to 400 mV s^{-1} and expressed as current *versus* potential *vs.* Ag/AgCl; the inset shows the cathodic and anodic peak current (I_{pc} and I_{pa}, respectively) as a function of the square root of the scan rate.

effective surface area of our nanocomposite electrode was computed as 0.332 cm^2. Thus, a large increase in the charging current within the ±1.0 V voltage range at the nanocomposite electrode is consistent with the increase in the conducting surface area of the f-MWCNT–PF nanocomposite electrode and the electrical conductivity of CNT.

The effect of applying different scan rates on the redox process of the Fe^{2+}/Fe^{3+} system was also investigated. Voltammograms obtained at different scan rates are shown in Fig. 7. The peak currents (I_{pa} and I_{pc}) in Fig. 7 increase with the scan rate (50–400 mV s^{-1}) and shift to more positive potentials. The current increases linearly with the square root of the scan rate ($\nu^{1/2}$) in the range of 50–400 mV s^{-1} (Fig. 7, inset), indicating diffusion-controlled behavior of the nanocomposite electrode. The fitting equations are:

$$I_{pa}\ (\mu A) = 260.72 + 65.58\nu^{1/2};\ R^2 = 0.983$$

$$I_{pc}\ (\mu A) = -549.92 - 66.263\nu^{1/2};\ R^2 = 0.9955$$

The shift in oxidation potential with the scan rate is an indication of system irreversibility.[65,66]

3.6.2 Impedance spectroscopic study of the f-MWCNT–PF nanocomposite and GOx–f-MWCNT–PF nanocomposite. We studied the stepwise assembly of the GOx–f-MWCNT–PF nanocomposite electrode (bioelectrode) using EIS measurements. EIS is an effective method to study surface modifications in an electrode.[64,67] Fig. 8 shows the impedance features, presented as Nyquist plots (Z_{imag} *vs.* Z_{real}) of the electrode before immobilization (a) and after immobilization (b) of GOx.

The Nyquist plots for the f-MWCNT–PF nanocomposite electrode and GOx–f-MWCNT–PF nanocomposite electrode are composed of low-frequency linear parts and high-frequency arc-shaped parts. A small arc in the high frequency region (Fig. 8a) is generally ascribed to a relatively low charge transfer resistance in the aqueous electrolyte. When GOx was immobilized on the functionalized electrode, the semicircle diameter increased (Fig. 8b), indicating that the modified film (bioelectrode) hindered the electron transfer of $[Fe(CN)_6]^{3-/4-}$. The electron transfer resistance (R_{ct}) of the f-MWCNT–PF nanocomposite electrode surface is 30.58 Ω. It increases to 161.2 Ω when GOx is immobilized on the surface by EDC–NHS chemistry. The low R_{ct} value of the f-MWCNT–PF nanocomposite electrode indicates that it acts as an excellent conducting interface and provides a favourable microenvironment for subsequent GOx immobilization at the surface. These data are consistent with the results obtained from CV experiments and demonstrate that GOx is successfully immobilized on the f-MWCNT–PF nanocomposite electrode and that the design of the electrochemical platform for glucose detection has been well depicted in Fig. 1.

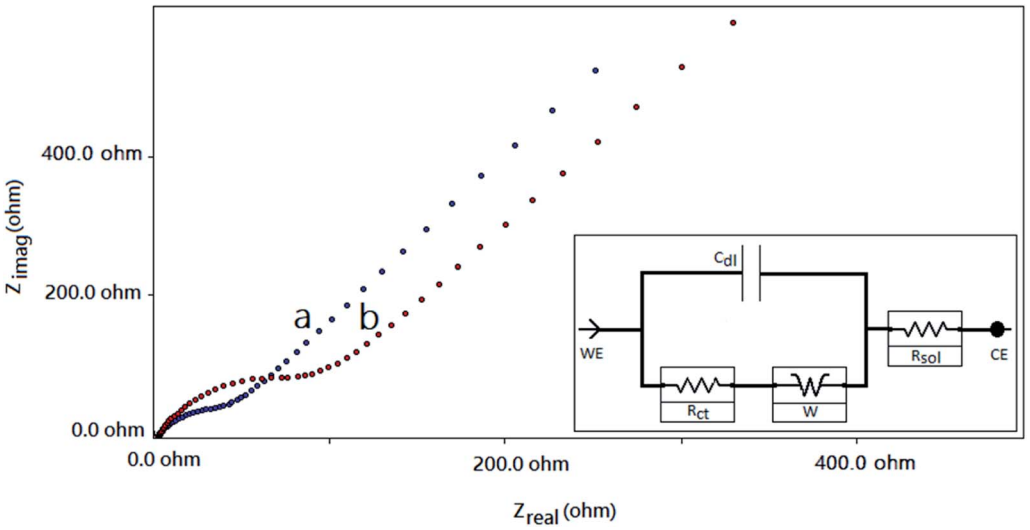

Fig. 8 EIS spectra of (a) the f-MWCNT–PF nanocomposite electrode and (b) the GOx–f-MWCNT–PF nanocomposite electrode in buffer solution. The inset shows the equivalent electrochemical cell circuit, which includes electron transfer, along with its equivalent circuit. C_{dl}, double-layer capacitance; R_{ct}, charge transfer resistance; R_{sol}, solution resistance; *W*, Warburg resistance.

3.6.3 Effect of pH. The solution pH is an important parameter for describing the electrochemical performance of a biosensing platform. The choice of an appropriate supporting electrolyte and its pH affects the redox behavior of the biochemical reaction and the biosensor sensitivity. This dependence is attributed to the protonation and deprotonation activity in the aqueous system, which affects the electron transfer process.[68] The effect of the pH of the supporting electrolyte on the analytical response of the bioelectrode was measured in the pH range of 5.0–8.0 in the presence of 5 mM of glucose as the analyte. The response of the GOx–f-MWCNT–PF nanocomposite electrode measured as anodic peak current (I_{pa}) with the pH of the medium is shown in Fig. 9a. GOx has optimum activity at pH 5.5. The anodic current–pH graph (Fig. 9b) also shows the maximum current density at pH 5.5. As shown in Fig. 9b, the maximum response peak current density with a GOx–f-MWCNT–PF nanocomposite electrode was found to decrease sharply above and below pH 5.5. Covalent immobilization thus does not alter the optimal pH of GOx. Protonation/deprotonation in the reaction medium affects the active site of immobilized GOx and the carboxylic functional groups present at the surface. The moderately high current response at pH 7.4 can be attributed to the dissociation of free/un-blocked carboxyl groups present at the CNT surface in the nanocomposite electrode. The cyclic voltammograms obtained at different pH values show only one oxidation peak and one reduction peak, confirming a one-electron-exchange reaction at the working electrode. Usually, a blood or blood serum sample is employed to measure blood glucose at the physiological pH of 7.4.[69] Therefore, it will be advantageous to test the performance of the proposed sensor in a pH 7.4 buffer solution, as used in the present study.

3.7 Analytical performance of the biosensor: calibration curve

The voltammetric response of the bioelectrode (GOx–f-MWCNT–PF nanocomposite electrode) was investigated using standard addition methods by successively adding glucose to 5 mL of PBS solution containing 5 mM ferricyanide solution $\{K_3[Fe(CN)_6]\}$ at room temperature. The reactions used for the measurement of glucose using fabricated bioelectrode can be described as follows:[70]

$$\text{Glucose} + GOx_{(ox)} \rightarrow \text{gluconic acid} + GOx_{(red)} \quad (A)$$

$$GOx_{(red)} + 2Fe^{3+} \rightarrow GOx_{(ox)} + 2Fe^{2+} + 2H^{+} \quad (B)$$

$$2Fe^{2+} \rightarrow 2Fe^{3+} + 2e^{-} \quad (C)$$

where $GOx_{(ox)}$ and $GOx_{(red)}$ represent the oxidized and reduced forms of glucose oxidase and Fe^{3+} and Fe^{2+} represent the oxidized and reduced forms of the mediator $\{K_3[Fe(CN)_6]\}$, respectively. The voltammograms obtained for different glucose concentrations are presented in Fig. 10(I) and (II). For the lower range, glucose concentrations with 0.08 mM (Fig. 10(Ia)), 0.1 mM (Fig. 10(Ib)), 0.4 mM (Fig. 10(Ic)), 0.5 mM (Fig. 10(Id)), 0.8 mM (Fig. 10(Ie)), 1 mM (Fig. 10(If)), 2 mM (Fig. 10(Ig)), and 4 mM (Fig. 10(Ih)) were used. For a higher glucose range, glucose concentrations of 5 mM (Fig. 10(IIa)), 10 mM (Fig. 10(IIb)), 15 mM (Fig. 10(IIc)), 20 mM (Fig. 10(IId)), 25 mM (Fig. 10(IIe)), 30 mM (Fig. 10(IIf)), and 35 mM (Fig. 10(IIg)) were prepared. From the voltammetric response, it was observed that the anodic current increases with the concentration of glucose, which confirms that the oxidation of glucose to gluconic acid is catalyzed by the enzyme GOx in the presence of ferricyanide as a mediator and generates the reduced form of the mediator, *i.e.* ferrocyanide $\{(K_4[Fe(CN)_6]\}$. Thus, the electrochemical signal produced by the oxidation of ferrocyanide released at the bioelectrode is used to quantify the glucose concentration present in the buffer solution.[70] The corresponding calibration curve [Fig. 10(III)] obtained from the well-defined current responses for glucose measured from the cyclic voltammetric current profiles exhibited two different regions of bioelectrode response behavior for glucose concentrations from 0.08 to 35.0 mM. The insets show the calibration plots obtained for the response to glucose at lower (A) and higher (B) concentrations

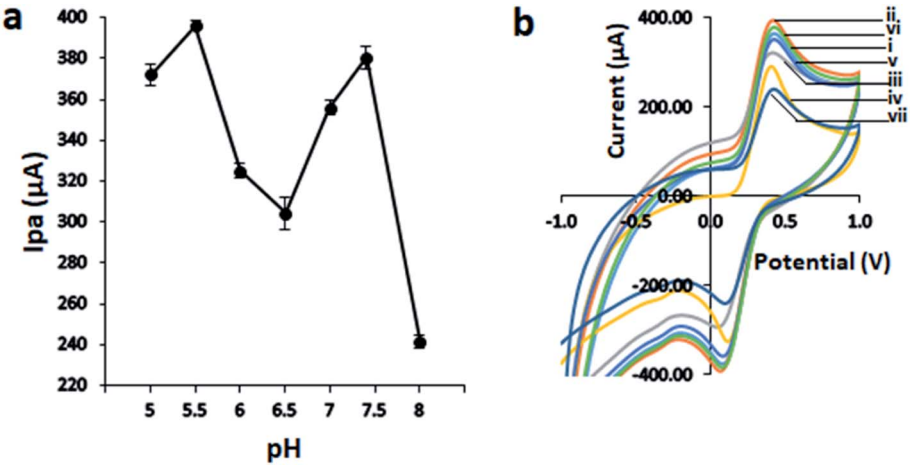

Fig. 9 Response of the bioelectrode at different pH values of buffer solution obtained from voltammetric measurements: (a) changes in the anodic peak current (I_{pa}) of the bioelectrode towards 5 mM glucose at different pH values, and (b) voltammograms obtained at different pH values: (i) 5, (ii) 5.5, (iii) 7, (iv) 6.5, (v) 6, (vi) 7.4, and (vii) 8.

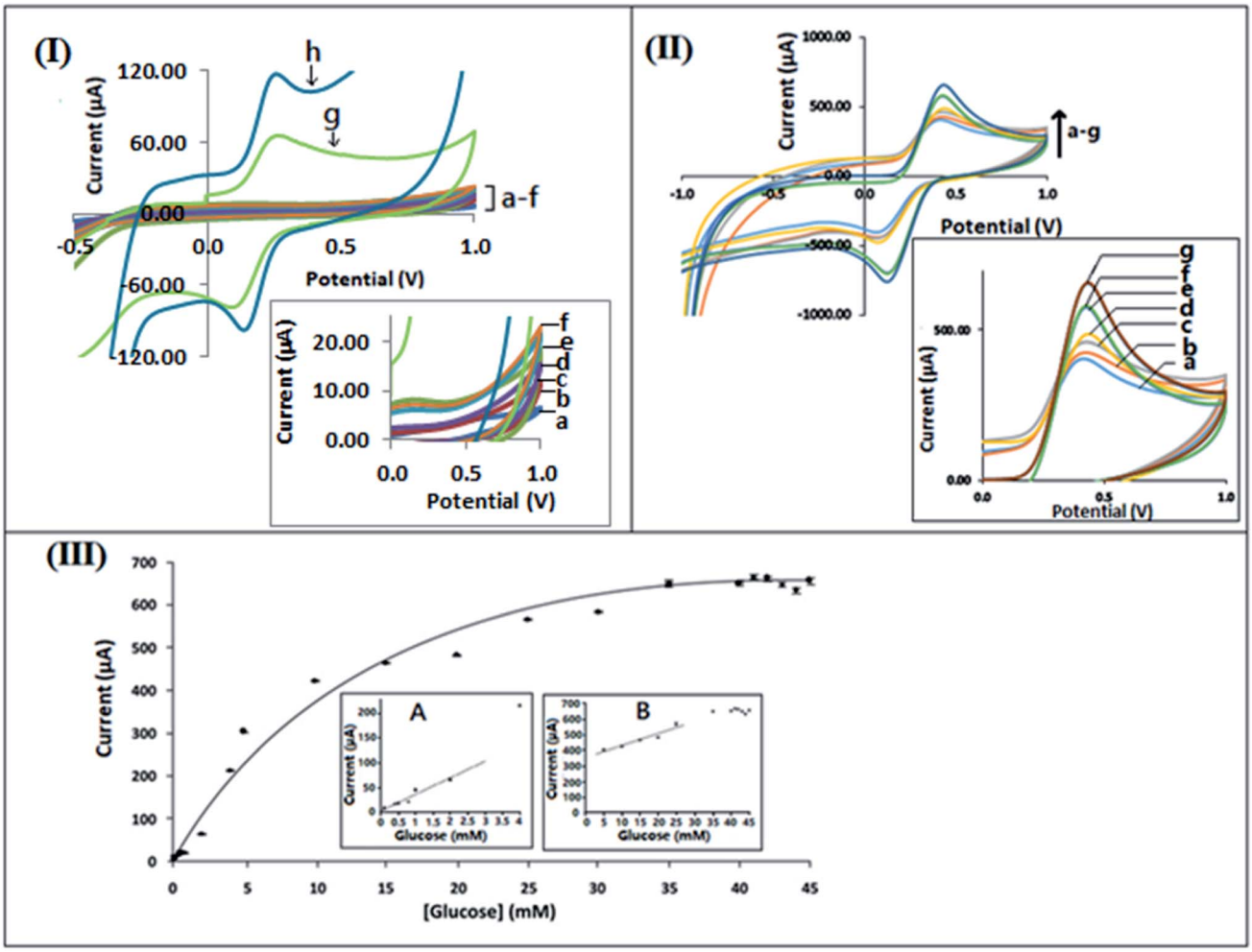

Fig. 10 Response of the GOx–f-MWCNT–PF nanocomposite bioelectrode to different glucose concentrations, obtained as: (I) voltammograms for glucose concentrations from 0.08 mM to 4 mM (a–h), with the inset showing the variations of the reduction current from (a–f); (II) voltammograms for glucose concentrations from 5 mM to 35 mM (a–g), with the inset showing the variations of the reduction current from (a–g); (III) calibration curve, with the insets showing (A) the calibration range from 0.08 mM to 4 mM (lower range); (B) the calibration range from 5.0 mM to 35 mM (higher range).

of glucose (details are given in the ESI data file as S4†). Thus, we found two regions of linear behavior: (A) 0.08 mM to 3 mM, with a correlation coefficient of 0.9723 and a sensitivity of 35.322 μA μM^{-1}; and (B) 5 mM to 35 mM, with a correlation coefficient of 0.9613 and a sensitivity of 9.346 μA mM^{-1}, represented by eqn (1) and (2), respectively:

$$I\,(\mu A) = 35.322\ [\text{glucose (mM)}] + 2.7983;\ R^2 = 0.9723 \quad (1)$$

$$I\,(\mu A) = 9.3462\ [\text{glucose (mM)}] + 333.78;\ R^2 = 0.9613 \quad (2)$$

The bioelectrode formed by immobilization of GOx onto the f-MWCNT–PF nanocomposite film shows uniform conductivity with an effective surface area 0.332 cm^2, possibly due to the homogeneous distribution of f-MWCNT on PF. The 3D intertwined MWCNT–PF network secures a constant sensitivity in the lower region of the calibration curve between 0.08 mM and 3 mM glucose concentration, represented by the accumulated points in the lower region of the calibration curve. The LOD values for the calibration curve are 0.03167 mM at a signal to noise ratio of 3. The capability of the bioelectrode for detection of the substrate at low concentration is essential for the development of wearable glucose sensor systems in which glucose can be measured from sweat, tears, or interstitial fluid above the dermis.[71–73] In the lower concentration region (0.08–3.0 mM) of the calibration curve, the sensitivity is lower, as the large density of GOx molecules immobilized at the electrode surface act as a barrier to electron transfer between the electrode surface and the solution interface, as reported in the literature.[74,75] The linear behavior found in the second region extends from 5 mM to 25 mM glucose concentration. The measurement of blood-glucose concentrations within these ranges can differentiate between a healthy and diabetic patient.[72]

3.8 Reproducibility, storage, and stability of the bioelectrode

The reproducibility of the proposed bioelectrode (GOx–f-MWCNT–PF nanocomposite electrode) during continuous operation was tested by measuring the decrease in the output signal (I_p) using

Table 2 Determination of glucose in blood serum samples using the proposed bioelectrode and a comparative spectrophotometric method used in clinical laboratories

S. no.	Concentration of glucose (mg dL^{-1}) (clinical method) (υ_E)	Concentration of glucose (mg dL^{-1}) (present method) (υ_A)	Relative error $\left[\frac{\upsilon_A - \upsilon_E}{\upsilon_E} \times 100\right]$
1	127	134.0014	5.5129
2	186	193.33	3.9408
3	250	264.450	5.78
4	211	224.054	6.1867
5	225	232.972	3.5431
6	96	98.2100	2.3020

5 mM of glucose solution in buffer solution (pH 7.4). The relative standard deviation (RSD) values obtained for the intraday and interday repeatability were 1.300427 ($n = 12$) and 1.511755 ($n = 12$), respectively, showing good accuracy for the measurements. This may be due to the stabilization of GOx at the CNT electrode surface by EDC–NHS immobilization, as reported earlier.[76]

Additionally, the reproducibility of the bioelectrode construction process was determined by measuring the response of three bioelectrodes prepared in different batches using the same procedure. The study was performed using 5 mM glucose solution measured in phosphate buffer solution (pH 7.4). Voltammetry was applied to measure the peak current (I_p) in triplicate, and the RSD was found to be within acceptable limits. The storage stability of the proposed bioelectrode was also examined in a buffer solution. It was found that after storage at 4 °C for 55 days, the sensor retained 95.0% of its initial current response. These results are considered to be acceptable and can be attributed to the conservation of the enzymatic activity, due to the effective immobilization of GOx on the CNT-based biocompatible support.[77]

3.9 Analytical application of the proposed method

The fabricated bioelectrode (GOx–f-MWCNT–PF electrode) was applied to determine the glucose concentrations in anonymized blood serum samples obtained from the hospital. The measurements were performed using standard addition methods in triplicate. The results obtained with our fabricated glucose-sensing bioelectrode and with the clinical method[78] are compared in Table 2.

The glucose content obtained with the present bioelectrode system was always higher than that measured by the clinical method, probably due to interference from other compounds present in blood serum. In healthy subjects, blood glucose levels are typically in the range of 4.9–6.9 mM, which increases up to 40 mM in diabetics after glucose intake.[79] The present study shows that our electrode is satisfactorily applicable to samples containing 5–25 mM (90.090–450.450 mg dL^{-1}) of blood glucose, with a relative error of not more than 6%. Thus, the bioelectrode-based measurement can differentiate a healthy person from a diabetic patient.

4. Conclusion

In summary, we have developed a f-MWCNT–PF nanocomposite with surface carboxylic functional groups which can act as a flexible, sheet-type universal electrochemical platform for the fabrication of enzyme-based electrochemical biosensors. The stepwise characterization of the bioelectrode fabrication process suggests that the oxidation of p-MWCNT by acidic oxidation does not break the internal structure of p-MWCNT and generates surface carboxylic functions that are essential for the development of CNT-ink and biomolecule immobilization. A stable dispersion of f-MWCNT in ethanol was created by sonication and was used as a CNT ink that is curable at room temperature. The thermal transfer of the CNT-ink onto a flexible PF surface generates the f-MWCNT–PF nanocomposite. Further, immobilization of GOx at the CNT surface yields a hybrid nanocomposite (GOx–f-MWCNT–PF) which can be directly used as a sheet-type flexible electrode for glucose sensing. The voltammetric calibration curve of the glucose biosensor shows two different linear regions of glucose response. The linear response of the biosensor between 0.08 mM and 2.0 mM indicates that our sensor platform can be effective for glucose sensing in sweat or interstitial fluid samples. As the nanocomposite is water repellent, flexible, and biocompatible, it can be directly integrated into the electronic components and the human body for continuous monitoring of other analytes that require waterproof platforms for analysis. We also demonstrated the potential application of the sensor in blood glucose measurement. Moreover, the relatively simple fabrication process of our sensor system is promising for mass production with uniform performance.

Author contributions

Rachana Sahney: conceptualization, funding acquisition, investigation, writing – original draft, designing experiment, methodology and supervised the project. Neha Gopal: investigation, writing – review & editing. Satish Kumar: assisted in the investigations and provided some constructive suggestions.

Conflicts of interest

There are no conflicts to declare.

Acknowledgements

We acknowledge the research funding from the Department of Biotechnology, India under the women scientist scheme to Rachana Sahney (research grants No. BT/Bio-CARe/05/640/2014-15); Department of Atomic Energy (DAE), Board of Research in

Nuclear Sciences (BRNS), India (research grants No. 37(2)/14/22/2017-BRNS/37219). We thank Dr A. K. Srivastava, Laboratory of Medicine, All India Institute of Medical Science, Delhi, India, for providing blood serum samples and their glucose analysis, which allowed us to compare our results with the clinical methods. Ethical clearance for the glucose estimation in blood serum was obtained from institutional ethical committee. Thanks are also due to Professor Irving R. Epstein for helpful discussions and English language correction.

References

1 M. Pumera, S. Sanchez, I. Ichinose and J. Tang, Electrochemical nanobiosensors, *Sens. Actuators, B*, 2007, **123**(2), 1195–1205.
2 S. Cosnier, Biomolecule immobilization on electrode surfaces by entrapment or attachment to electrochemically polymerized films. A review, *Biosens. Bioelectron.*, 1999, **14**(5), 443–456.
3 A. Le Goff, M. Holzinger and S. Cosnier, Enzymatic biosensors based on SWCNT-conducting polymer electrodes, *Analyst*, 2011, **136**(7), 1279–1287.
4 A. Heller, Electrical connection of enzyme redox centers to electrodes, *J. Phys. Chem.*, 1992, **96**(9), 3579–3587.
5 I. Willner and B. Willner, Biomaterials integrated with electronic elements: en route to bioelectronics, *Trends Biotechnol.*, 2001, **19**(6), 222–230.
6 R. Sahney, B. Puri and S. Anand, Enzyme coated glass pH-electrode: Its fabrication and applications in the determination of urea in blood samples, *Anal. Chim. Acta*, 2005, **542**(2), 157–161.
7 R. Sahney, S. Anand, B. Puri and A. Srivastava, A comparative study of immobilization techniques for urease on glass-pH-electrode and its application in urea detection in blood serum, *Anal. Chim. Acta*, 2006, **578**(2), 156–161.
8 R. Srivastava, R. Sahney, S. Upadhyay and R. Gupta, Membrane permeability based cholesterol sensor—A new possibility, *J. Membr. Sci.*, 2000, **164**(1–2), 45–49.
9 G. Jeevanandham, R. Jerome, N. Murugan, M. Preethika, K. Vediappan and A. K. Sundramoorthy, Nickel oxide decorated MoS_2 nanosheet-based non-enzymatic sensor for the selective detection of glucose, *RSC Adv.*, 2020, **10**(2), 643–654.
10 G. Jeevanandham, K. Vediappan, Z. A. ALOthman, T. Altalhi and A. K. Sundramoorthy, Fabrication of 2D-$MoSe_2$ incorporated NiO nanorods modified electrode for selective detection of glucose in serum samples, *Sci. Rep.*, 2021, **11**(1), 1–13.
11 Q. Zhai and W. Cheng, Soft and stretchable electrochemical biosensors, *Materials Today Nano*, 2019, **7**, 100041.
12 S. Shrivastava, N. Jadon and R. Jain, Next-generation polymer nanocomposite-based electrochemical sensors and biosensors: A review, *TrAC, Trends Anal. Chem.*, 2016, **82**, 55–67.
13 D. Son and Z. Bao, Nanomaterials in skin-inspired electronics: Toward soft and robust skin-like electronic nanosystems, *ACS Nano*, 2018, **12**(12), 11731–11739.
14 N. Matsuhisa, X. Chen, Z. Bao and T. Someya, Materials and structural designs of stretchable conductors, *Chem. Soc. Rev.*, 2019, **48**(11), 2946–2966.
15 U. Yogeswaran and S. M. Chen, Recent trends in the application of carbon nanotubes–polymer composite modified electrodes for biosensors: A review, *Anal. Lett.*, 2008, **41**(2), 210–243.
16 S. Merum, J. B. Veluru and R. Seeram, Functionalized carbon nanotubes in bio-world: applications, limitations and future directions, *Mater. Sci. Eng., B*, 2017, **223**, 43–63.
17 M. Sireesha, V. Jagadeesh Babu, A. S. Kranthi Kiran and S. Ramakrishna, A review on carbon nanotubes in biosensor devices and their applications in medicine, *Nanocomposites*, 2018, **4**(2), 36–57.
18 P. Serp and E. Castillejos, Catalysis in carbon nanotubes, *ChemCatChem*, 2010, **2**(1), 41–47.
19 E. M. Remillard, Z. Branson, J. Rahill, Q. Zhang, T. Dasgupta and C. D. Vecitis, Tuning electric field aligned CNT architectures via chemistry, morphology, and sonication from micro to macroscopic scale, *Nanoscale*, 2017, **9**(20), 6854–6865.
20 D. H. Youn, G. Bae, S. Han, J. Y. Kim, J.-W. Jang, H. Park, *et al.*, A highly efficient transition metal nitride-based electrocatalyst for oxygen reduction reaction: TiN on a CNT–graphene hybrid support, *J. Mater. Chem. A*, 2013, **1**(27), 8007–8015.
21 L. Li and Y. Xing, Methanol electro-oxidation on Pt–Ru alloy nanoparticles supported on carbon nanotubes, *Energies*, 2009, **2**(3), 789–804.
22 D. Tasis, N. Tagmatarchis, A. Bianco and M. Prato, Chemistry of carbon nanotubes, *Chem. Rev.*, 2006, **106**(3), 1105–1136.
23 N. Gopal, P. Shukla and R. Sahney, Development of CNT–polymer film-based electrode for the detection of glucose, *Advances in Polymer Sciences and Technology*, Springer, 2018, pp. 177–186.
24 B. V. Basheer, J. J. George, S. Siengchin and J. Parameswaranpillai, Polymer grafted carbon nanotubes—Synthesis, properties, and applications: A review, *Nano-Struct. Nano-Objects*, 2020, **22**, 100429.
25 N. Mohd Nurazzi, M. Muhammad Asyraf, A. Khalina, N. Abdullah, F. A. Sabaruddin, S. H. Kamarudin, *et al.*, Fabrication, Functionalization, and Application of Carbon Nanotube-Reinforced Polymer Composite: An Overview, *Polymers*, 2021, **13**(7), 1047.
26 K. Zhang, B. Han and X. Yu, Electrically conductive carbon nanofiber/paraffin wax composites for electric thermal storage, *Energy Convers. Manage.*, 2012, **64**, 62–67.
27 C. Li and H. Yang, Expanded vermiculite/paraffin composite as a solar thermal energy storage material, *J. Am. Ceram. Soc.*, 2013, **96**(9), 2793–2798.
28 F. C. Moraes, D. L. Golinelli, L. H. Mascaro and S. A. Machado, Determination of epinephrine in urine using multi-walled carbon nanotube modified with cobalt phthalocyanine in a paraffin composite electrode, *Sens. Actuators, B*, 2010, **148**(2), 492–497.

29 Parafilm M, Product Numbers-P 7793, Sigma Aldrich, 3050 Spruce Street, Saint Louis, Missouri, 63103, USA, https://www.sigmaaldrich.com/IN/en/product/sigma/p7793.
30 Y. Hokama, R. S. Lane and J. A. Howarth, Maintenance of adult and nymphal *Ornithodoros coriaceus* (Acari: Argasidae) by artificial feeding through a parafilm membrane, *J. Med. Entomol.*, 1987, **24**(3), 319–323.
31 S. Javaherian, K. A. O'Donnell and A. P. McGuigan, A fast and accessible methodology for micro-patterning cells on standard culture substrates using Parafilm™ inserts, *PLoS One*, 2011, **6**(6), e20909.
32 M. Ewens and P. Felker, The potential of mini-grafting for large-scale production of *Prosopis alba* clones, *Journal of Arid Environments*, 2003, **55**(2), 379–387.
33 P. Gaskin, J. MacMillan, R. Firn and R. Pryce, "Parafilm": A convenient source of *n*-alkane standards for the determination of gas chromatographic retention indices, *Phytochemistry*, 1971, **10**(5), 1155–1157.
34 L. Yu and Z. Z. Shi, Microfluidic paper-based analytical devices fabricated by low-cost photolithography and embossing of Parafilm®, *Lab Chip*, 2015, **15**(7), 1642–1645.
35 S. Higham and W. Edgar, Effects of Parafilm® and cheese chewing on human dental plaque pH and metabolism, *Caries Res.*, 1989, **23**(1), 42–48.
36 L. Valentini, S. B. Bon, M.-A. Lopez-Manchado, L. Mussolin and N. Pugno, Development of conductive paraffin/graphene films laminated on fluoroelastomers with high strain recovery and anti-corrosive properties, *Compos. Sci. Technol.*, 2017, **149**, 254–261.
37 J. E. Mates, I. S. Bayer, J. M. Palumbo, P. J. Carroll and C. M. Megaridis, Extremely stretchable and conductive water-repellent coatings for low-cost ultra-flexible electronics, *Nat. Commun.*, 2015, **6**(1), 1–8.
38 N. Sezer and M. Koç, Oxidative acid treatment of carbon nanotubes, *Surf. Interfaces*, 2019, **14**, 1–8.
39 M. A. Aegerter and M. Mennig, *Sol–gel technologies for glass producers and users*, Springer Science & Business Media, 2013.
40 J. Schönherr, J. R. Buchheim, P. Scholz and P. Adelhelm, Boehm titration revisited (part i): Practical aspects for achieving a high precision in quantifying oxygen-containing surface groups on carbon materials, *C*, 2018, **4**(2), 21.
41 Y. Gao and I. Kyratzis, *Covalent immobilization of proteins on carbon nanotubes using the cross-linker 1-ethyl-3-(3-dimethylaminopropyl)carbodiimide—a critical assessment*, ACS Publications, 2008.
42 S. K. Soni, B. Thomas and V. R. Kar, A Comprehensive Review on CNTs and CNT-Reinforced Composites: Syntheses, Characteristics and Applications, *Mater. Today Commun.*, 2020, 101546.
43 M. Trojanowicz, Analytical applications of carbon nanotubes: a review, *TrAC, Trends Anal. Chem.*, 2006, **25**(5), 480–489.
44 J. M. Schnorr and T. M. Swager, Emerging applications of carbon nanotubes, *Chem. Mater.*, 2011, **23**(3), 646–657.
45 J. Sandler, J. Kirk, I. Kinloch, M. Shaffer and A. Windle, Ultra-low electrical percolation threshold in carbon-nanotube–epoxy composites, *Polymer*, 2003, **44**(19), 5893–5899.
46 Y. Lin, S. Taylor, H. Li, K. S. Fernando, L. Qu, W. Wang, *et al.*, Advances toward bioapplications of carbon nanotubes, *J. Mater. Chem.*, 2004, **14**(4), 527–541.
47 J. Wang, Carbon-nanotube based electrochemical biosensors: A review, *Electroanalysis*, 2005, **17**(1), 7–14.
48 N. Gopal, A. Saxena and R. Sahney, Effect of functionalization on the electrochemical behavior of multi-walled carbon nanotube and parafilm nanocomposites, *Fullerenes, Nanotubes, Carbon Nanostruct.*, 2021, **29**(8), 643–655.
49 I. Mazov, V. L. Kuznetsov, I. A. Simonova, A. I. Stadnichenko, A. V. Ishchenko, A. I. Romanenko, *et al.*, Oxidation behavior of multiwall carbon nanotubes with different diameters and morphology, *Appl. Surf. Sci.*, 2012, **258**(17), 6272–6280.
50 R. Arrigo, R. Teresi, C. Gambarotti, F. Parisi, G. Lazzara and N. T. Dintcheva, Sonication-induced modification of carbon nanotubes: Effect on the rheological and thermo-oxidative behaviour of polymer-based nanocomposites, *Materials*, 2018, **11**(3), 383.
51 Y. Yan, J. Miao, Z. Yang, F.-X. Xiao, H. B. Yang, B. Liu, *et al.*, Carbon nanotube catalysts: recent advances in synthesis, characterization and applications, *Chem. Soc. Rev.*, 2015, **44**(10), 3295–3346.
52 K. A. Wepasnick, B. A. Smith, K. E. Schrote, H. K. Wilson, S. R. Diegelmann and D. H. Fairbrother, Surface and structural characterization of multi-walled carbon nanotubes following different oxidative treatments, *Carbon*, 2011, **49**(1), 24–36.
53 Y. Peng and H. Liu, Effects of oxidation by hydrogen peroxide on the structures of multiwalled carbon nanotubes, *Ind. Eng. Chem. Res.*, 2006, **45**(19), 6483–6488.
54 A. Bucio, R. Moreno-Tovar, L. Bucio, J. Espinosa-Dávila and F. Anguebes-Franceschi, Characterization of beeswax, candelilla wax and paraffin wax for coating cheeses, *Coatings*, 2021, **11**(3), 261.
55 H. Edwards and M. Falk, Fourier-transform Raman spectroscopic study of unsaturated and saturated waxes, *Spectrochim. Acta, Part A*, 1997, **53**(14), 2685–2694.
56 T. A. Iida, K. Honda and H. Nozaki, Identification of normal paraffins and olefins from thermal decomposition products of polyethylene, *Bull. Chem. Soc. Jpn.*, 1973, **46**(5), 1480–1482.
57 N. T. Dintcheva, R. Arrigo, C. Gambarotti, S. Carroccio, G. Filippone, F. Cicogna, *et al.*, α-Tocopherol-induced radical scavenging activity in carbon nanotubes for thermo-oxidation resistant ultra-high molecular weight polyethylene-based nanocomposites, *Carbon*, 2014, **74**, 14–21.
58 E. Y. Malikov, M. B. Muradov, O. H. Akperov, G. M. Eyvazova, R. Puskás, D. Madarász, *et al.*, Synthesis and characterization of polyvinyl alcohol based multiwalled carbon nanotube nanocomposites, *Phys. E*, 2014, **61**, 129–134.
59 M. R. Nejadnik, F. L. Deepak and C. D. Garcia, Adsorption of Glucose Oxidase to 3-D Scaffolds of Carbon Nanotubes:

Analytical Applications, *Electroanalysis*, 2011, **23**(6), 1462–1469.

60 H. Zhao and H. Ju, Multilayer membranes for glucose biosensing via layer-by-layer assembly of multiwall carbon nanotubes and glucose oxidase, *Anal. Biochem.*, 2006, **350**(1), 138–144.

61 R. L. McCreery, Advanced carbon electrode materials for molecular electrochemistry, *Chem. Rev.*, 2008, **108**(7), 2646–2687.

62 S. Sánchez, M. Pumera and E. Fàbregas, Carbon nanotube/polysulfone screen-printed electrochemical immunosensor, *Biosens. Bioelectron.*, 2007, **23**(3), 332–340.

63 K. Gong, S. Chakrabarti and L. Dai, Electrochemistry at carbon nanotube electrodes: Is the nanotube tip more active than the sidewall?, *Angew. Chem.*, 2008, **120**(29), 5526–5530.

64 A. J. Bard and L. R. Faulkner, *Fundamentals and applications. Electrochemical Methods*, 2001, vol. 2(482), pp. 580–632.

65 D. Martín-Yerga, E. Costa Rama and A. Costa García, Electrochemical study and determination of electroactive species with screen-printed electrodes, *J. Chem. Educ.*, 2016, **93**(7), 1270–1276.

66 X. Yang, W. Yuan, D. Li and X. Zhang, Study on an improved bio-electrode made with glucose oxidase immobilized mesoporous carbon in biofuel cells, *RSC Adv.*, 2016, **6**(29), 24451–24457.

67 A. R. Bredar, A. L. Chown, A. R. Burton and B. H. Farnum, Electrochemical impedance spectroscopy of metal oxide electrodes for energy applications, *ACS Appl. Energy Mater.*, 2020, **3**(1), 66–98.

68 D. H. Evans, Solution electron-transfer reactions in organic and organometallic electrochemistry, *Chem. Rev.*, 1990, **90**(5), 739–751.

69 Y. Lin, F. Lu, Y. Tu and Z. Ren, Glucose biosensors based on carbon nanotube nanoelectrode ensembles, *Nano Lett.*, 2004, **4**(2), 191–195.

70 J. Wang, Electrochemical glucose biosensors, *Chem. Rev.*, 2008, **108**(2), 814–825.

71 J. R. Windmiller and J. Wang, Wearable electrochemical sensors and biosensors: a review, *Electroanalysis*, 2013, **25**(1), 29–46.

72 H. Yao, A. J. Shum, M. Cowan, I. Lähdesmäki and B. A. Parviz, A contact lens with embedded sensor for monitoring tear glucose level, *Biosens. Bioelectron.*, 2011, **26**(7), 3290–3296.

73 D. Bruen, C. Delaney, L. Florea and D. Diamond, Glucose sensing for diabetes monitoring: recent developments, *Sensors*, 2017, **17**(8), 1866.

74 B.-C. Kang, B.-S. Park and T.-J. Ha, Highly sensitive wearable glucose sensor systems based on functionalized single-wall carbon nanotubes with glucose oxidase–nafion composites, *Appl. Surf. Sci.*, 2019, **470**, 13–18.

75 J. Mohapatra, B. Ananthoju, V. Nair, A. Mitra, D. Bahadur, N. Medhekar, *et al.*, Enzymatic and non-enzymatic electrochemical glucose sensor based on carbon nano-onions, *Appl. Surf. Sci.*, 2018, **442**, 332–341.

76 J. Ge, J. Lei and R. N. Zare, Protein–inorganic hybrid nanoflowers, *Nat. Nanotechnol.*, 2012, **7**(7), 428–432.

77 C. Wang, Q. Wang and R. Tan, Preparation of enzyme-functionalized carbon nanotubes and their application in glucose and Fe^{2+} detection through "turn on" and "turn off" approaches, *Analyst*, 2018, **143**(17), 4118–4127.

78 P. Trinder, Glucose assay: a colorimetric enzyme-kinetic method assay, *Ann. Clin. Biochem.*, 1969, **6**, 24.

79 Z. Zhou, Z. Zhu, F. Cui, J. Shao and H. S. Zhou, CuO/Cu composite nanospheres on a TiO_2 nanotube array for amperometric sensing of glucose, *Microchim. Acta*, 2020, **187**(2), 1–8.